PLASMA DYNAMICS

V. PLASMAS AND CONTROLLED NUCLEAR FUSION*

A. Waves and Radiation

Academic and Research Staff

Prof. G. Bekefi	Prof. B. Coppi	Dr. R. Gajewski
Prof. W. P. Allis	Prof. W. M. Manheimer	Dr. P. A. Politzer
Prof. A. Bers	Prof. B. L. Wright	J. J. McCarthy
Prof. S. C. Brown		W. J. Mulligan

Graduate Students

R. J. Becker	H. Bhattacharya	L. P. Mix, Jr.
E. L. Bernstein	A. J. Cohen	L. D. Pleasance
	L. Litzenberger	

1. RECENT DEVELOPMENTS IN THE STUDY OF ION ACOUSTIC WAVES

The theory for the propagation of ion acoustic waves is usually based on either the Vlasov equation or the transport, or moment, equations. In this report a hybrid theory is presented. In this theory we use the transport equations to describe the ion dynamics, and the Vlasov equation to describe the electron dynamics. The predictions of this theory are then compared with recent observations of ion acoustic waves. These observations differ from those previously reported[1] in that the wave damping shows a strong dependence on the frequency, with very little damping present at the higher frequencies. The damping at the higher frequencies is found to be in very good agreement with that predicted by a Vlasov description of both species. The damping at the lower frequencies appears to be explainable only by a more complicated theory which would be valid in the transition region where the assumptions of both the Vlasov and hybrid theories break down.

Motivation for the development of a hybrid theory of ion acoustic waves was furnished by the failure of the collisionless theory to explain the experimentally observed heavy damping at low frequencies. Because the electron-electron, electron-ion and electron-neutral collision mean-free paths are much longer than the main vacuum chamber of PF 1, the Vlasov equation was chosen to describe the electron dynamics. The ion-ion mean-free paths are typically less than a few centimeters; therefore, at least at low enough frequencies, the transport equations should give an accurate description of the ion dynamics. For these reasons, the hybrid theory appeared to be an appropriate description of the low-frequency ion acoustic wave behavior.

*This work was supported by the U.S. Atomic Energy Commission (Contract AT(30-1)-3980).

Using this model, we shall obtain the dispersion relations by first solving the respective ion and electron equations for the normal-mode density fluctuations of the two species and then coupling the density fluctuations through Poisson's equation. As previously noted,[1,2] these waves appear to propagate as plane waves along the magnetic field because they show no ion-cyclotron cutoff. Therefore, the equations will be linearized in one dimension, and the electrostatic approximation will be assumed.

An expression for the electron density fluctuations is now obtained from the Vlasov equation.

$$\frac{\partial f}{\partial t} + \vec{v} \cdot \frac{\partial}{\partial \vec{x}} f + \vec{a} \cdot \frac{\partial}{\partial \vec{v}} f = 0. \tag{1}$$

This equation is linearized by assuming that the distribution function, f, comprises the sum of an equilibrium Maxwellian distribution, f_o, and a small perturbation, f_1, having a space-time dependence of the form $e^{-i\omega t+ikz}$. The normalization of f_o is defined by the following equation in one dimension:

$$\int f_o \, dv_z = 1. \tag{2}$$

Making use of these approximations and the assumptions in Eq. 1, we obtain

$$f_1 = \frac{-ieE}{m_e k} \left(\frac{\frac{\partial f_o}{\partial v}}{v - \frac{\omega}{k}} \right), \tag{3}$$

where e is the charge of a proton, E is the self-consistent electric field, and m_e is the mass of the electron. Defining

$$\alpha_e^2 = \frac{2T_e}{m_e}, \tag{4}$$

where T_e is the electron temperature, we obtain for n_{e_1}, the electron density perturbation,

$$\frac{n_{e_1}}{n_o} = \int f_1 \, dv_z = \frac{-ieE}{m_e k \alpha_e^2} Z' \left(\frac{\frac{\omega}{k} - V_e}{\alpha_e} \right), \tag{5}$$

where Z' is the derivative of the plasma dispersion function, n_o is the steady-state density, and V_e is the electron drift velocity.

An expression for the ion density fluctuations is now obtained from the transport, or moment, equations. Braginskii[3] has considered these equations in some detail; therefore, the transport equations, as well as the transport coefficients, that he presents will be

used in this derivation. It should be noted that although the transport coefficients may be derived by several methods, each method assumes that the local distribution is close to a Maxwellian. A necessary condition, therefore, for the use of these coefficients is that the variations in space and time be slow enough to allow the local distribution to remain near a Maxwellian. These restrictions may be written in the following forms:

$$\frac{\partial}{\partial x} \sim k < \frac{1}{\lambda_i}$$

$$\frac{\partial}{\partial t} \sim \omega < \nu_i, \tag{6}$$

where ν_i and λ_i are the ion-ion collision frequency and mean-free path, respectively. With these restrictions in mind, we now consider the transport equations of Braginskii, where the subscript i is omitted for simplicity.

$$\frac{\partial n}{\partial t} + \vec{\nabla} \cdot (n\vec{v}) = 0. \tag{7}$$

$$mn \frac{d}{dt} v_\alpha = -\frac{\partial p}{\partial x_\alpha} - \frac{\partial}{\partial x_\beta} \pi_{\alpha\beta} + en\left(E_\alpha + \left(\frac{\vec{v}}{c} \times \vec{B}\right)_\alpha\right) - R_\alpha \tag{8}$$

$$\frac{3}{2} n \frac{d}{dt} T + p(\vec{\nabla} \cdot \vec{v}) = -\vec{\nabla} \cdot \vec{q} - \pi_{\alpha\beta} \frac{\partial}{\partial x_\beta} v_\alpha + Q. \tag{9}$$

In these equations the ions are assumed to obey the ideal gas law, $p_i = n_i T_i$, d/dt is the convective derivative, and $\pi_{\alpha\beta}$ is a stress tensor which, in the absence of a magnetic field, is given by

$$\pi_{\alpha\beta} = -\eta_o \left(\frac{\partial v_\alpha}{\partial x_\beta} + \frac{\partial v_\beta}{\partial x_\alpha} - \frac{2}{3} \delta_{\alpha\beta} \vec{\nabla} \cdot \vec{v}\right), \tag{10}$$

where the subscript i is omitted. The viscous coefficient, η_o, is given by the following equation for singly ionized particles:

$$\eta_o = 0.96 \frac{n_i T_i}{\nu_i}. \tag{11}$$

The term $\vec{R}$ is the sum of the thermal force exerted on the ions by collisions with electrons and a friction force caused by streaming of the ions and electrons at different velocities. In one dimension this force has the form

$$R_z = -0.71 n_e \frac{\partial}{\partial z} T_e - 0.51 m_e n_e \nu_e (V_e - V_i). \tag{12}$$

Again the coefficients are for single ionized particles. In this derivation this term is neglected because of the long electron-ion and electron-electron mean-free paths. The

vector $\vec{q}$ is a heat flux vector which in one dimension has the form

$$q_z = -3.9 \frac{n_i T_i}{m_i \nu_i} \frac{\partial}{\partial z} T_i. \tag{13}$$

The term Q_i represents the heat acquired by ions in collisions with electrons and is represented by

$$Q_i = \frac{3m_e}{m_i} n_e \nu_e (T_e - T_i). \tag{14}$$

As is $\vec{R}$, this term is neglected in this derivation. The ion-neutral mean-free path is typically much longer than a wavelength; therefore, the effects of neutrals on the ion dynamics have been neglected.

We assume that the ion density, velocity, and temperature are sums of a zero-order average value and a small first-order perturbation having a space-time dependence of the form $e^{-i\omega t+ikz}$. Substituting these expansions in Eqs. 7-9 and collecting terms that are linear in perturbation quantities, we obtain three additional equations which, when combined, yield the following equation for the ion density perturbation:

$$\frac{n_{i_1}}{n_o} = \frac{\frac{iekE}{m_i}}{\omega^*(\omega^*+1.28\gamma) - \frac{k^2 T_i}{m_i}\left(1 + \frac{2/3\,\omega^*}{\omega^* + 2.6\gamma}\right)}, \tag{15}$$

where

$$\omega^* = \omega - kV_i$$

$$\gamma = i \frac{k^2 T_i}{m_i \nu_i}.$$

The electron and ion density perturbations can now be related in a self-consistent manner through Poisson's equation.

$$\vec{\nabla} \cdot \vec{E} = 4\pi n_o e \left(\frac{n_{i_1}}{n_o} - \frac{n_{e_1}}{n_o}\right). \tag{16}$$

Using Eqs. 5 and 15 for the density perturbations, we obtain the dispersion relation

$$1 - \frac{\omega_{p_i}^2}{\omega^*(\omega^*+1.28\gamma) - \frac{k^2 T_i}{m_i}\left(1 + \frac{2/3\,\omega^*}{\omega^* + 2.6\gamma}\right)} - \frac{\omega_{p_e}^2}{k^2 a_e^2} Z'\left(\frac{\frac{\omega}{k} - V_e}{a_e}\right) = 0. \tag{17}$$

Using the assumptions of Eq. 6 and assuming $T_e \gg T_i$, $|\omega/k - V_e| \ll a_e$ and $\omega = \omega_r + i\omega_i$, we obtain the approximate solution of Eq. 17.

$$\omega_r = k\left(\sqrt{\frac{T_e + \frac{5}{3}T_i}{m_i}} + V_i\right) \tag{18}$$

$$\frac{\omega_i}{\omega_r} = -0.64\,\frac{T_i}{T_e}\sqrt{\frac{T_e}{m_i}}\,\frac{k}{\nu_i} - \sqrt{\frac{\pi}{8}}\sqrt{\frac{m_e}{m_i}}. \tag{19}$$

In the equation for the damping ω_i, the drift velocities are neglected. Exact numerical solutions of Eq. 17 have shown very good agreement with Eqs. 18 and 19 with variations typically less than 10%.

Ion acoustic waves recently observed have shown striking differences from those previously reported.[1] These waves show a strong variation of the damping with frequency, as well as greatly reduced damping at the higher frequencies, with values of $\omega_i/\omega_r = -0.015$ sometimes observed. These waves are observed at pressures a factor of two higher than normally used. The launching and detection systems are similar to those shown in a previous report.[1] The only major modification has been the substitution of a doubly balanced crystal mixer for the gated amplifier in order to suppress the carrier from the driving signal. Also each grid has been changed from a fine tungsten mesh to three 0.65-mil tungsten wires crossed to form an asterisk-shaped grid. The wave potential variations are observed by floating the receiving grid with respect to ground. The transmitting grid is also floated.

The results of these measurements are shown in Fig. V-1, where both $D_e/\lambda = -\omega_r/2\pi\omega_i$ and ω_r are plotted as a function of k. Theoretical curves are also presented in Fig. V-1. These curves are obtained from the numerical solutions of Eq. 17 in this report and from Eq. 2 in a previous report.[2] The value of the ion drift velocity used in these calculations is obtained from later upstream-downstream wave propagation measurements. The electrons are assumed to drift at the same velocity. The value of the density is estimated from probe curve measurements. The values of T_e and T_i are chosen to give a good fit of the Vlasov theory to the observed high-frequency wave data. The value of T_e so chosen is in reasonable agreement with the value obtained from probe curve measurements. The value of T_i is somewhat higher than the parallel ion temperature, $T_{i_\parallel}$, measured by Silk[4] in PF2; but it is lower than the perpendicular ion temperature, $T_{i_\perp}$, which he measured. Because of the short mean-free paths for ion-ion collisions in PF 1 and PF 2, an isotropic velocity distribution is expected for the ions. It is reasonable to expect this isotropic distribution to have a temperature between the values of $T_{i_\parallel}$ and $T_{i_\perp}$ measured by Silk.

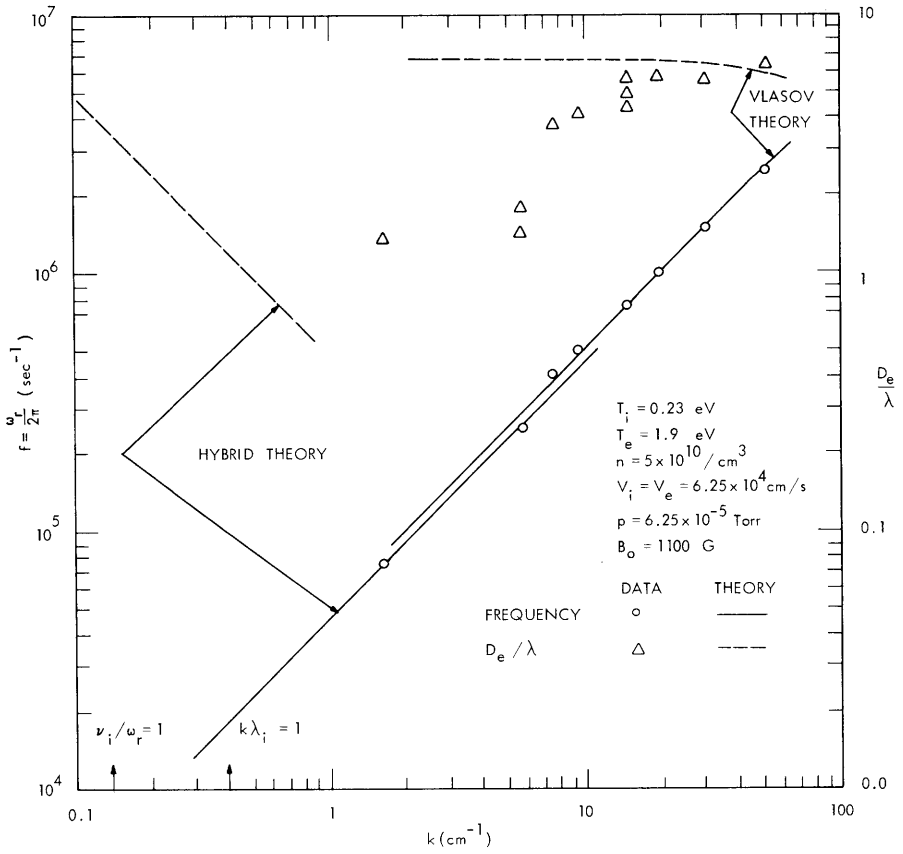

Fig. V-1. Experimental and theoretical dispersion curves for an Argon plasma.

It is interesting to note that the slight break in the real part of the experimental dispersion relation occurs at about the same value of k as the break in the imaginary part. Although the break in the real part has always been observed in previous dispersion plots, this marks the first observation of a distinct break in the damping data.

L. P. Mix, Jr., L. Litzenberger

References

1. L. P. Mix, Jr., L. Litzenberger, and G. Bekefi, Quarterly Progress Report No. 93, Research Laboratory of Electronics, M. I. T., April 15, 1969, pp. 69-72.
2. L. P. Mix, Jr. and G. Bekefi, Quarterly Progress Report No. 94, Research Laboratory of Electronics, M. I. T., July 15, 1969, pp. 89-98.
3. S. I. Braginskii, in Reviews of Plasma Physics, M. A. Leontovich (ed.) (Consultants Bureau Enterprises, Inc., New York, 1965), Vol. 1, pp. 205-311.
4. J. K. Silk, Quarterly Progress Report No. 93, Research Laboratory of Electronics, M. I. T., April 15, 1969, pp. 111-116.

2. LONGITUDINAL PROFILES IN ARGON PLASMAS IN PLASMA FACILITY 1 (PF 1)

Considerable effort has been devoted to the study[1] of the plasmas generated in PF 1 and PF 2. We shall report here on one phase of this study, namely the investigation of the longitudinal profiles of the ion density, floating potential, space potential, electron temperature, and ion drift velocity in Argon plasmas in PF 1. Among other things, this investigation provided information about the relative importance of volume ionization and ionization within the Lisitano structure itself. It also provided a partial explanation for the appreciable ion drifts previously reported.[2]

First we shall discuss the most relevant features of the experimental arrangement. Three grids were interposed in the plasma column, with their planes perpendicular to the column. Each of the two grids nearest the Lisitano structure were composed of three 0.65-mil tungsten wires, crossed equiangularly at the center of a 2-in. stainless-steel ring on which they were mounted. We chose this combination of wire diameter and configuration in the hope that it would result in very little plasma perturbation. These two grids were used as transmitter and receiver during the ion acoustic wave observations; and the second of these two grids, the one that was farther from the structure, was used as a longitudinally movable probe during the rest of the observations.

The third grid was made of 5.5-mil stainless-steel mesh with approximately 80 wires per inch, and was supported by a 2-in. stainless-steel ring. This grid was positioned far enough from the end of the main vacuum chamber to be in the uniform region of the magnetic field. This grid served to define a surface of constant potential within the uniform-field region. The value of the potential was externally controllable; for all but one set of data this grid was grounded. The interwire distance was chosen small enough to ensure that the Debye length was always greater than one-tenth of the interwire distance. We refer to this grid as the "collector grid."

Eighteen solenoids were present. All but the first two were connected in series. A mirror ratio of approximately 1.12 was always employed. The magnetic field values reported below are those of the uniform field. Data were taken only in the uniform-field region.

The amount of power incident on the structure always was between 42 W and 48 W; however, the amount of reflected power varied much more from one set of data to another, possibly because of changes in impedance matching as we varied the frequency of the microwave power. The structure, which was grounded, was always located approximately in that region where the magnetic field increases from the uniform-field value to its maximum value.

Of the three diffusion pumps that are part of PF 1, only that one located farthest

from the microwave structure was employed. The neutral gas pressure read on the ionization gauge directly above this pump was approximately 3.4×10^{-5} Torr for all data. Pressures from 2 1/2 to 3 times this value were read on the ionization gauge at the center manifold.

The wave-launching and wave-detection systems used during the ion acoustic wave observations were similar to those described in a previous report.[3] The only major change in the launching system was the substitution of a doubly balanced crystal mixer for the gated amplifier. This substitution was made in order to suppress the carrier. The transmitting and receiving grids were floated with respect to ground, and typically a few rms volts of signal was applied to the transmitting grid. The modulation frequency was 100 Hz, and the carrier frequency typically was 753 kHz.

The externally controllable parameters that were varied most from one set of data to the next were the magnetic field and, correspondingly, the frequency of the microwave power which was incident on the structure. Initially, we had hoped to gain insight into the diffusion processes in PF 1 by varying the magnetic field. This hope was only partially realized because of the complications arising out of the volume ionization that was observed at certain field values.

Each density profile shown in Fig. V-2 was obtained by biasing the middle grid into the ion saturation region and by measuring the ion saturation current as this grid was moved longitudinally by means of a motor-drive system. These current values were related in the following manner to the average density values which are plotted on the y-axis: for each set of data, at 4 or 5 different longitudinal positions we measured the current drawn by this grid as a function of the voltage applied to it. We found that the current had the same functional dependence on the voltage as in the case of a conventional cylindrical Langmuir probe. Consequently, we applied the theory for a conventional cylindrical probe[4] to the grid-probe curves to determine an average ion density, electron temperature, and space potential. An effective probe length of 6 in. was assumed. Comparing the average density obtained in this manner with the values of the ion saturation current that we measured at the same longitudinal positions, we found that the current values were so nearly linearly proportional to these average density values for each set of data that we could fairly and easily select a value for the constant of proportionality. Also, we found that this constant did not vary appreciably from one set of data to another; consequently, we thought it both reasonable and desirable to compute the average of these constants and to use this average to change the y-axis variable in Fig. V-2 from ion saturation current to average density.

By observing both waves propagating toward the microwave structure and waves propagating away from this structure, the ion drift velocity $\vec{v}_D$ and $T_e + 3T_i$ can be measured, where T_e and T_i are the electron and ion temperatures, respectively.[5] For each set of data we examined the waves at three or fewer different longitudinal positions.

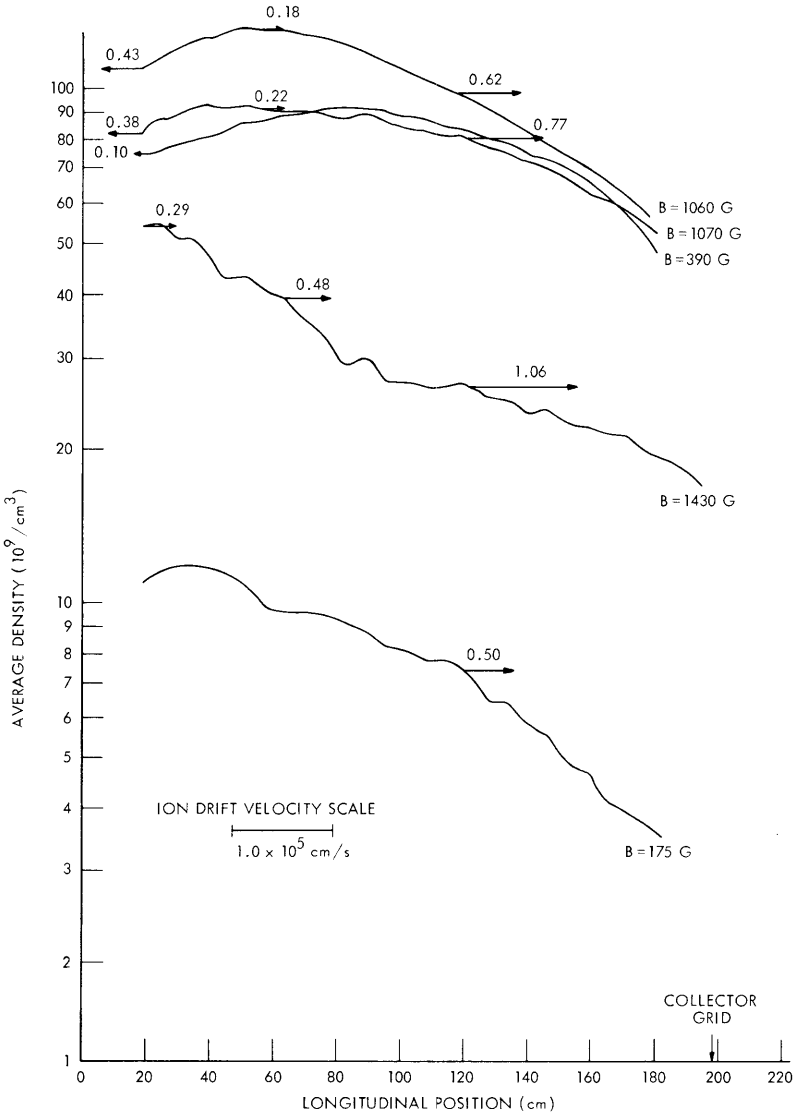

Fig. V-2. Longitudinal density profiles in Argon plasmas. The longitudinal positions are relative to the nearer end of the Lisitano structure. The measured ion drift velocities are indicated by arrows.

Each drift velocity thus measured is indicated in Fig. V-2 by an arrow, the length of which is proportional to the magnitude of the velocity and the direction of which specifies the direction of the velocity. Each arrow is attached to the appropriate profile.

In Fig. V-3 the longitudinal profiles of the floating and space potentials are displayed. Each floating potential curve was obtained by connecting the middle grid to a high impedance voltmeter and by moving this grid longitudinally by means of the motor-drive system. Each space potential curve is a smooth curve drawn through the four or five data points that we obtained by using the grid-probe curves referred to above. Both the floating and space potential values are relative to the potential applied to the collector

grid. This grid was grounded except for the data at 1060 G, in which case this grid was biased at +25 V. The number T^* is the average value of $T_e + 3T_i$ obtained from the wave data.

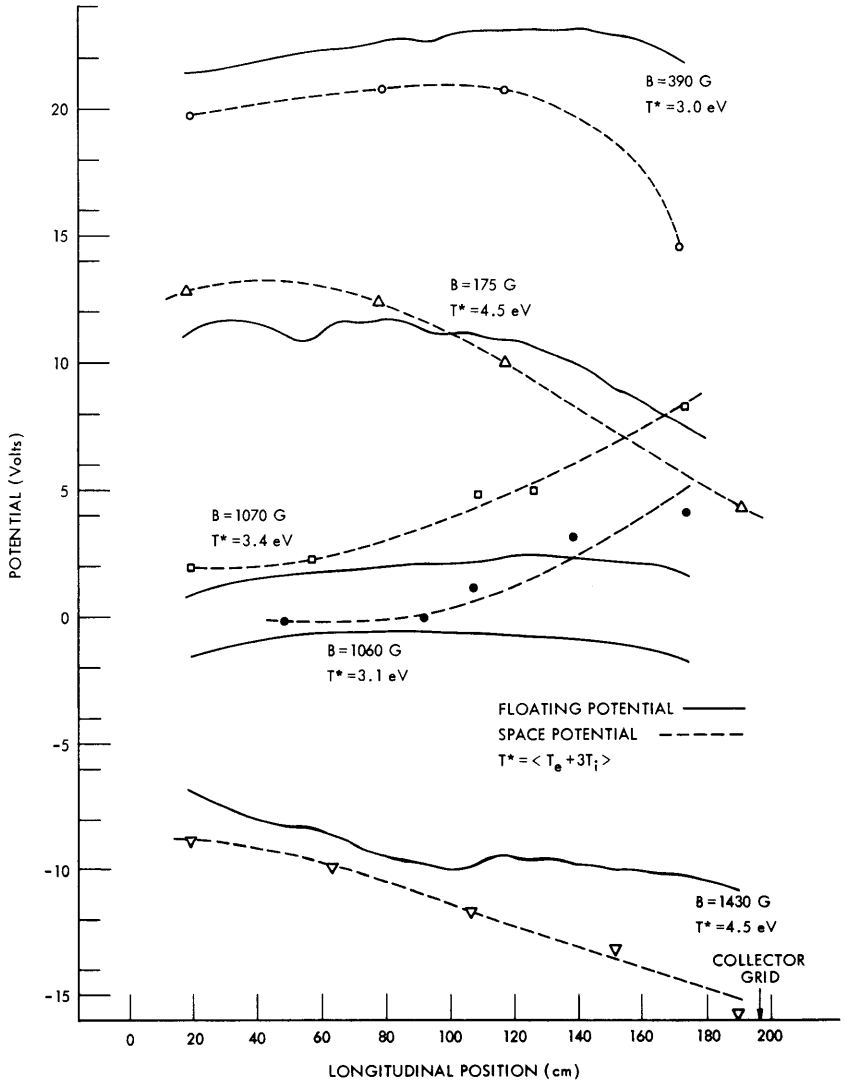

Fig. V-3. Longitudinal potential profiles in Argon plasmas. The longitudinal positions are relative to the nearer end of the Lisitano structure. The potentials are relative to the potential applied to the collector grid.

Now let us note some features of the longitudinal profiles. In general, the deeper the potential well for the electrons in the longitudinal direction, the more symmetric is the density profile. (The one exception to this trend – the data at 175 G – may be due to increased radial diffusion losses resulting from the relative weakness of the magnetic field.) In the one case in which a large potential well for ions is observed, a

monotonically decreasing density profile is seen. We conclude from these observations that volume ionization may become important relative to the ionization occurring inside the Lisitano structure itself, when a well for electrons exists. This conclusion is reasonable because such a well appears necessary in order to have appreciable volume ionization in PF 1, where the mean-free paths for ionization are longer than the length of the main vacuum chamber. Dreicer and McLeod[6] have suggested volume ionization as a plasma-production mechanism in electron-cyclotron heating machines. As an aside, we might note that the density and potential profiles have somewhat similar shapes in general.

We see that the three most symmetric density profiles correspond to the most dense plasmas. It may be unfair, however, to claim this as additional evidence of volume ionization because we expect that the amount of ionization occurring inside the Lisitano structure itself depends upon how close to resonance the magnetic field is tuned.

We note that the ion drift velocity and the density gradient typically are in opposite directions in Fig. V-2. This suggests that the drift velocity may be related to the density gradient through the equation $n\vec{v}_D = -D\vec{\nabla}n$, where n is the density, and D is a "diffusion coefficient." We find this to be the case for the data at 1060 G and 1070 G, when we subtract from each drift velocity a velocity vector equal to the drift velocity observed in the region of the plasma where $\vec{\nabla}n = 0$. This subtracted velocity may be attributable to that portion of the plasma which is produced inside the Lisitano structure and streams out of the structure with a net velocity. The value of D – approximately 7×10^6 cm^2/sec – is observed to be close to the value of $v_{th_i}^2/\nu_{in}$, where v_{th_i} is the ion thermal speed, and ν_{in} is the ion-neutral collision frequency. This suggests that ion-neutral collisions may be an important mechanism in the axial diffusion process.

On the other hand, the drift velocity data at 1430 G cannot be related to the density gradient through the equation $n\vec{v}_D = -D\vec{\nabla}n$. Furthermore, a free-fall theory for the ions in conjunction with the observed potential profiles cannot explain this drift velocity data. A more sophisticated model appears to be necessary in this case.

Almost without exception, the value of $T_e + 3T_i$ obtained from the wave data increases with increasing distance from the microwave structure. The over-all increases are between 10% and 20%. The values of T_e from the grid-probe curves do not show any general trend with longitudinal position.

L. Litzenberger, L. P. Mix, Jr., G. Bekefi

References

1. J. K. Silk, Ph. D. Thesis, Department of Physics, M. I. T., August 1969; L. P. Mix, Jr., E. W. Fitzgerald, and G. Bekefi, Quarterly Progress Report No. 92, Research Laboratory of Electronics, M. I. T., January 15, 1969, p. 227.

2. L. N. Litzenberger, S. M. Thesis, Department of Physics, M.I.T., June 1969, p. 22.

3. L. P. Mix, Jr., L. Litzenberger, and G. Bekefi, Quarterly Progress Report No. 93, Research Laboratory of Electronics, M. I. T., April 15, 1969, p. 69.

4. L. P. Mix, Jr., E. W. Fitzgerald, and G. Bekefi, Quarterly Progress Report No. 92, Research Laboratory of Electronics, M. I. T., January 15, 1969, pp. 231-233.

5. See Eq. (4) in L. P. Mix, Jr., and G. Bekefi, Quarterly Progress Report No. 94, Research Laboratory of Electronics, M. I. T., July 15, 1969, p. 89.

6. H. Dreicer and J. McLeod, Status Report of the LASL Controlled Thermonuclear Research Program for 12-month period ending October 31, 1967, Report LA-3831-MS, Los Alamos Scientific Laboratory of the University of California, p. 21.

V. PLASMAS AND CONTROLLED NUCLEAR FUSION*

C. Plasma Diagnostics

Academic and Research Staff

Prof. G. Bekefi
Prof. B. L. Wright
Dr. E. V. George
Dr. P. A. Politzer

Graduate Students

L. D. Pleasance

1. HIGH-PRESSURE PULSED CO_2 LASER

The production of dense hot plasmas by means of powerful lasers has been known for many years. The study of these plasmas was difficult partly because of the sophisticated laser technology that is required and partly because of the very slow repetition rate of these devices and their lack of reproducibility. For these reasons, careful plasma diagnostics could only be made on single shots and the rate of gathering information (because of the slow repetition rate) was very tedious. We shall describe the construction of a pulsed CO_2 laser that alleviates most of these drawbacks.

One of the main disadvantages of previous CO_2 lasers is that the peak Q-switched power is small for a workable-sized laser. For example, the 200 KW (peak power) laser used by Smith and Haught[1] required an oscillator and a multipass amplifier that was several meters long. Work on CO_2 lasers has now proceeded to the point where it is relatively easy to achieve multimegawatt laser pulses at high repetition rates with components of high reliability and low cost. These lasers also operate at or near atmospheric pressure, thereby reducing the need for high-vacuum components.

This laser is not only useful in producing high-density plasmas, by optical breakdown, but is also useful as a source of high-intensity, electromagnetic fields for studies of optical satellites. It has been shown that the intensity of an optical satellite is directly proportional to the peak power of the incident radiation (see, for example, George[2]). In our previous work the laser's peak power was ~10 kW. This resulted in a marginal signal-to-noise ratio. An increase in power to 1 MW would result in a signal increase of approximately two orders of magnitude. For these reasons, we decided to construct the high-pressure CO_2 laser described in this report.

The type of laser that was constructed was first discussed in a brief note by J. A. Beaulieu.[3] The excitation scheme comprises numerous simultaneous transverse electrical discharges distributed uniformly along the resonant cavity. This method of

*This work was supported by the U.S. Atomic Energy Commission (Contract AT(30-1)-3980).

excitation achieves population inversion rapidly and gain switching gives rise to giant-pulse operation automatically without need for Q switching. In order to maintain a fairly uniform distribution of discharge along the laser cavity the discharge electrodes are resistively loaded.

Our laser has a series of 171, 1.1 kΩ, 0.5 W, carbon composition resistors spaced 3/16" apart on Plexiglas tubing, 2 in. OD × 34 in. long. The use of carbon or metal film resistors is avoided because they tend to explode when the discharge is initiated. The resistor leads act as cathodes. The anode is a polished brass rod, 3/8 in. in diameter. The gap between the anode and cathodes is 1 in. The tubing is fitted with salt flat Brewster windows, and the optical cavity is formed by using a 5-M radius of maximum curvature reflector and a dielectric coated 10-M radius of curvature 65% reflectance output mirror. The mirror separation is ~1.5M.

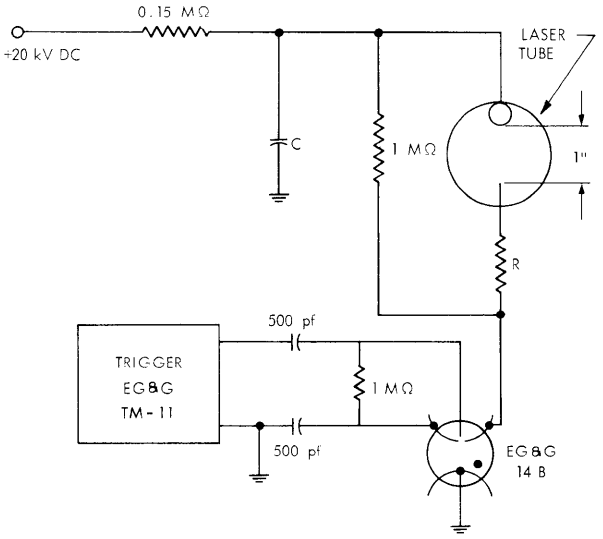

Fig. V-4. Electrical schematic for the CO_2 laser. The value of C is optimized at 0.03 μf. Only one of the 171 cathode resistors, R, is shown. Each is a 1.1 kΩ, 0.5 W, carbon composition resistor.

The discharge is produced by charging a capacitor to ~20 kV and then discharging it through the laser tube via the spark gap. The electrical circuit for the laser is illustrated in Fig. V-4. The laser discharge appears to operate best with fast-rising current pulses; therefore, care is taken to minimize the inductance of the discharge circuit. This is accomplished by placing the capacitor and spark gap as close as possible to the laser tube. The value of the capacitance, C, is optimized for maximum laser

output at 0.03 μF. Laser action occurs for values of C between approximately 0.01 and 0.05 μF.

The laser output is studied by using a liquid-nitrogen-cooled Au-doped Ge detector. This detector has a rise time of approximately 20 ns. Figure V-5 illustrates both the

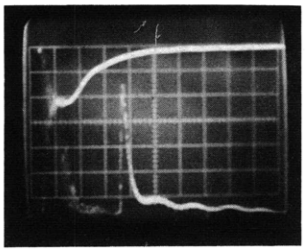

Fig. V-5.

Upper trace: Inverted current pulse, 250 a/div.
Lower trace: Detector output 0.2 V/div.
Time is increasing toward the right 0.5 μsec/div, for a mixture ratio 1:1:12, supply voltage 20 kV, and a gas pressure ~350 Torr.

laser discharge current pulse and laser output pulse as a function of time as seen on a dual-beam Tektronix Type 556 oscilloscope. The CO_2:N_2:He mixture ratio is 1:1:12 at total gas pressure of ~350 Torr (note that for photographic purposes the current is inverted). One sees from this figure that giant-pulse laser action occurs in the plasma afterglow some ~0.5 μs after the current pulse has occurred. In some instances a second laser pulse occurs some 1-2 μs after the first laser pulse. The mode pattern of the laser output appears quite complicated in the unapertured maximum-power operation. The mode pattern is rectangular, approximately 3/4 cm wide × 2 cm high. No major effort has yet been made to run the laser in a single mode.

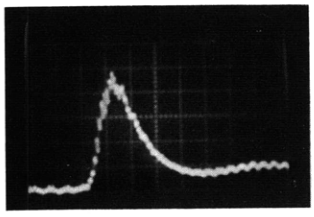

Fig. V-6.

Detector output, 0.2 V/div, as a function of time, 100 nsec/div for the laser operating conditions cited for Fig. V-5.

Figure V-6 illustrates the laser output pulse for the same operating conditions as in Fig. V-5 on an expanded time scale, as seen on a 150-MHz, Tektronix Type 454 oscilloscope. From this figure we obtain a pulse width of ~150 ns, after making corrections for the rise time of the detector. The energy in this pulse was measured with a TRG Model 100 thermopile and was found to be 0.17 J. This yields a laser peak power of ~1.1 MW. When the reflectivity of the output mirror is lowered to 35% a laser pulse, ~75 ns wide, is obtained. The energy in this pulse, however, was much lower

than the other one. The structure of the pulse, as illustrated in Fig. 6, suggests the onset of self-mode locking, which is common to many of the glass and ruby laser systems; however, this structure is thought to arise because of impedance mismatches in the detector cables.

This laser is pulsed at a repetition rate of 10 pps. The upper limit on the repetition rate is limited by the power rating of the cathode resistors and the de-ionization time of the spark gap. Rates as high as 1000 pps have been quoted.[3]

The variation of the average laser power output for different discharge voltages is illustrated in Fig. V-7 for several gas pressures. The CO_2:N_2:He mixture ratio is 1:1:12, with a total flow rate of ~300 atm-cc/min. The laser is repetitively pulsed at

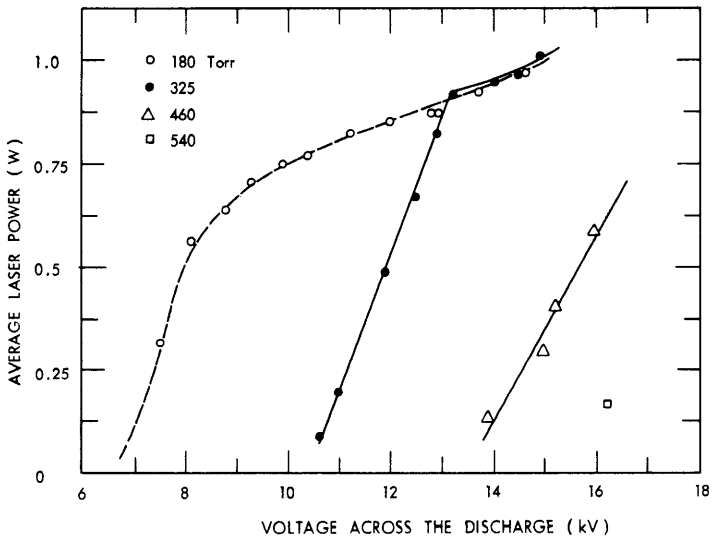

Fig. V-7. Variation of the average laser power with discharge voltage for several gas pressures. The laser is pulsed at a rate of 8 pps and the CO_2:N_2:He mixture ratio is 1:1:12.

8 pps and the average power is measured with a Coherent Radiation Laboratories Model 201 power meter. The breaks in the curves occur at the onset of the formation of constricted arc current filaments in the laser discharge at several of the resistor legs. When these filaments are fully formed even the carbon composition resistors tend to explode. In general, data are taken only in pressure, mixture, and voltage regions where this problem is minimal.

The electrical characteristics of the discharge from a single cathode as a function of the voltage across the discharge for the lowest operating pressure are illustrated in Fig. V-8. Notice that the breaks in the curves occur at the same voltage as that in Fig. V-7.

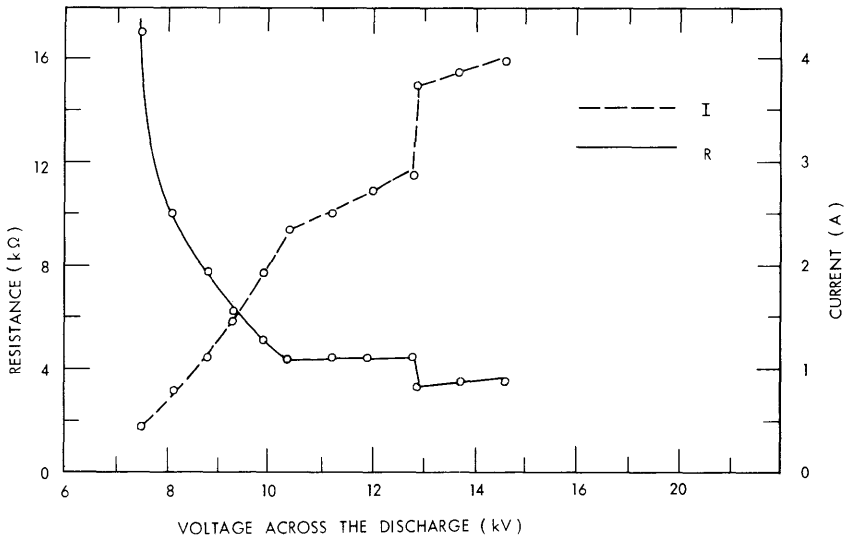

Fig. V-8. Electrical characteristics of the discharge from a single cathode as a function of the voltage across the discharge for a 180-Torr gas pressure.

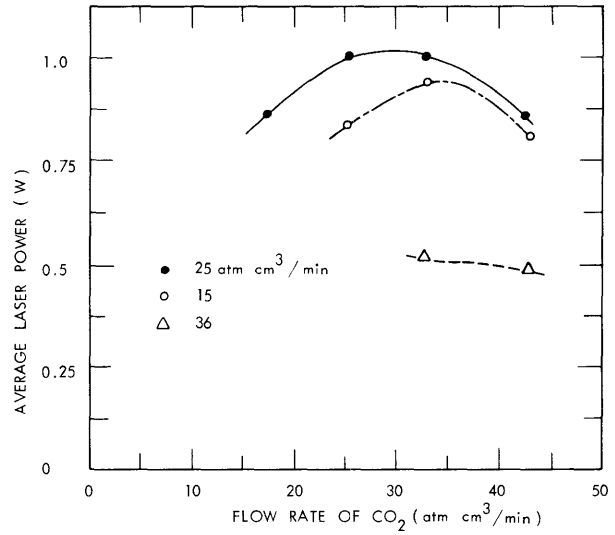

Fig. V-9. Dependence of the average laser output power on the $CO_2:N_2:He$ mixture ratio. The supply voltage is 20 kV, the laser repetition rate is 8 pps, and the He flow rate is 320 atm cm^3/min.

Figure V-9 illustrates the dependence of the average laser output power on the CO_2:N_2:He mixture ratio. The supply voltage is 20 kV, and the operating pressure range was 330-390 mm Hg. For these measurements the He flow rate is held constant at 320 atm.-cc/min, and the N_2 and CO_2 flow rates varied. We see that for a supply voltage of 20 dV the optimum mixture ratio is 1:1:12.

The output of this laser when focused will produce optical breakdown of gases and solids. The high-density plasma thus produced is found to be reproducible shot-to-shot within several percent. This permits simple temporal and spatial diagnostics. Moreover, it should be possible, in the future, to use synchronous detection techniques in those cases in which the signal-to-noise ratio is marginal. Initial studies of the optical spectra of such laser-produced plasmas are reported in Section V-C.2.

E. V. George, L. D. Pleasance

References

1. D. C. Smith and A. F. Haught, "Investigation of the Mechanisms Associated with Gas Breakdown under Intense Optical Illumination," Final Report F920272-12, prepared under Contract Nonr-4696(00) for the Office of Naval Research, December 1967.

2. E. V. George, M. Pawlak, G. Bekefi, and B. Ya'akobi, Quarterly Progress Report No. 96, Research Laboratory of Electronics, M.I.T., January 15, 1970, pp. 103-108.

3. A. Beaulieu, "Atmospheric-Pressure CO_2 Laser," Laser Focus, p. 14, February 1970.

2. OPTICAL SATELLITES INDUCED IN A PLASMA THROUGH THE ACTION OF INTENSE, HIGH-FREQUENCY ELECTRIC FIELDS

We are continuing our study of the optical satellites induced in a plasma through the action of intense high-frequency electric fields. Several modifications of the experimental arrangement have been made since our last report.[1] The 10-kW, Q-switched CO_2 laser, has been replaced by a pulsed high-pressure CO_2 laser described in Sec. V-C. 1, and a 1. 5-m film spectrometer incorporated into the experiment. The present experimental arrangement is illustrated in Fig. V-10. The 0. 5-m scanning spectrometer, together with the gated boxcar integrator is being used to study the time dependence of the spectral lines from laser-produced plasmas. This laser-produced plasma is generated by means of the pulsed CO_2 laser. The laser radiation is focused by means of a lens, of 3. 8 cm focal length, onto a cylindrical post of lithium, housed in a cell containing helium as a buffer gas. The lithium post is rotated continuously to prevent excessive pitting of the surface by the laser pulses. The radiation from the intense plasma plume thus generated is studied by means of a 1. 5-m spectrometer, focused on a small section of the plasma. Excellent spatial resolution of ~0. 1 mm is achieved so that the spatial plasma profile can be readily observed.

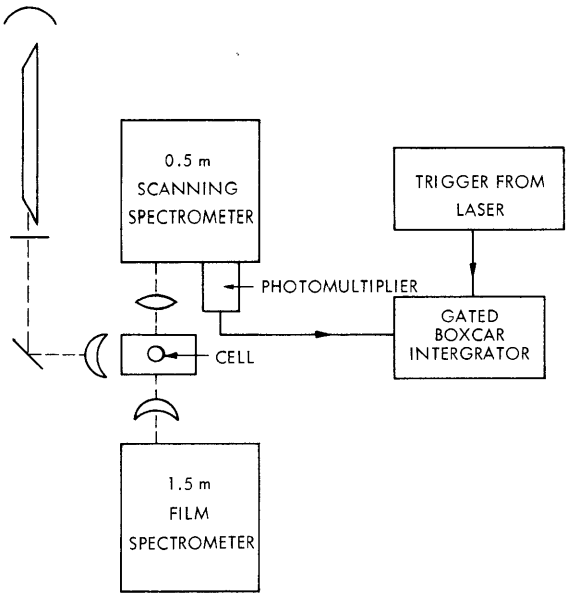

Fig. V-10. Experimental arrangement.

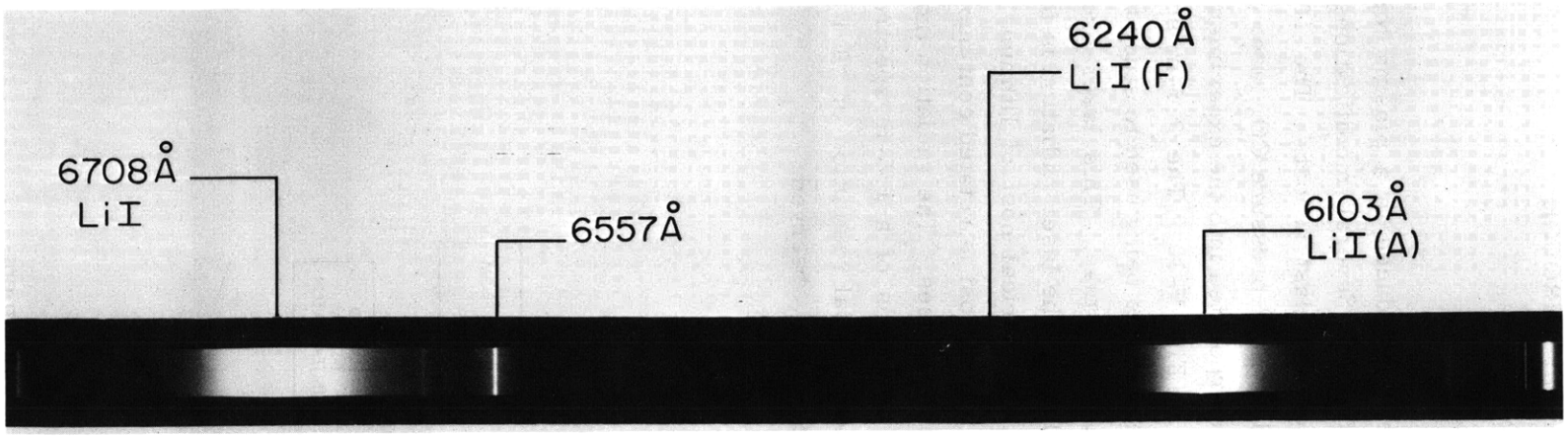

Fig. V-11. Spectrum of a laser-produced lithium plasma. A is the allowed line, F the forbidden line.

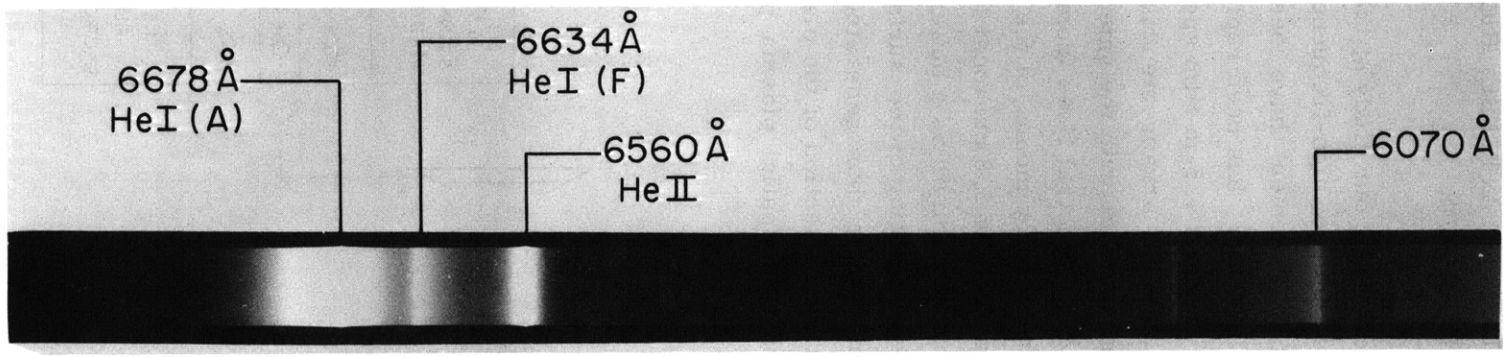

Fig. V-12. Spectrum of a laser-produced He plasma. The He pressure is 1 atm, A is the allowed line, F the forbidden line.

A representative spectrogram of this plasma is illustrated in Fig. V-11. The spectrogram exhibits the allowed 2P-3D line (A) and the 2P-3D forbidden line. Thus far, the plasma satellites have not yet been seen.

We have also studied the plasma generated by the optical breakdown of He gas at atmospheric pressure. A representative spectrogram of this plasma exhibiting the allowed 3D-2P line (A) and the 3P-2P forbidden line is shown in Fig. V-12. The skewed nature of the forbidden line is to be expected and is now being studied theoretically.

Thus far, the satellites induced by the electric field of the CO_2 laser, which also generates the plasma, have not been seen. This could be due to the fact that in the early times of the plasma, when the laser is present, the plasma is almost fully ionized; hence, there are not enough neutral atoms present for the forbidden line or the satellites to appear. This has been verified by time-resolved intensity measurements of the He 3P-2P forbidden line.

E. V. George, M. Pawlak, G. Bekefi

References

1. E. V. George, M. Pawlak, G. Bekefi, and B. Ya'akobi, Quarterly Progress No. 96, January 15, 1970, pp. 103-108.

V. PLASMAS AND CONTROLLED NUCLEAR FUSION*

E. High-Temperature Toroidal Plasmas

Academic and Research Staff

Prof. B. Coppi	Prof. R. A. Blanken	Prof. R. R. Parker
Dr. D. B. Montgomery†	Prof. R. J. Briggs	Prof. K. I. Thomassen
Prof. G. Bekefi	Prof. L. M. Lidsky	Dr. R. Gajewski
Prof. A. Bers	Prof. W. M. Manheimer	Dr. P. A. Politzer

1. ANOMALOUS RESISTIVITY AND TOKAMAK REGIMES

During our visit to the I. V. Kurchatov Institute of Atomic Energy, in 1967, Artsimovich presented the results of an effort that had been made to obtain electron temperature values for Tokamak plasmas (TM-3 device) by two independent methods, The criticism raised at the 1965 Culham conference on the validity of the temperature values reported there by the Kurchatov group had motivated this study.

The two independent methods consisted in deducing the electron temperature from the measured electrical resistivity and from diamagnetic measurements of the plasma pressure. The results showed that for applied electric fields E larger than, or of the order of, the run-away field E_{run} the measured resistivity (that is, the ratio of the applied electric field to the average measured current) was higher than that computed by the Spitzer classical resistivity formula with the measured diamagnetic temperature used in it.[1] The novelty of the observation consisted in the fact that for the considered plasmas, the electron cyclotron frequency Ω_e was larger than the electron plasma frequency ω_{pe}. In fact, anomalous resistivity higher than classical, which is due only to the effects of electron-ion collisions, was previously known to appear for regimes where $\omega_{pe} > \Omega_e$.

An interpretation of this observation was proposed by Kadomtsev and Pogutze.[2] Their argument was that when the electron distribution function acquires a sufficiently high tail of run-away electrons, in the direction of the electric field, parallel to the main magnetic field B, pitch angle scattering attributable to wave-particle interactions can take place. As a result of this, a significant group of fast particles with relatively large transverse velocity is formed, and Kadomtsev and Pogutze's point was that these particles would be responsible for the measured diamagnetic pressure.

The relevant wave-particle resonance, the so-called anomalous Doppler effect, is respresented by

$$\omega - \Omega_e + k_{||} v_{||} = 0, \tag{1}$$

*This work was supported by the U.S. Atomic Energy Commission (Contract AT(30-1)-3980).

†Dr. D. Bruce Montgomery is at the Francis Bitter National Magnet Laboratory.

where $v_{||}$ is the electron parallel velocity, Ω_e the gyro frequency, ω the wave frequency, and $k_{||}$ the wave number. Since $\omega < \omega_{pe} < \Omega_e$, Eq. 1 reduces to $k_{||}v_i \approx \Omega_e$, so that the energy exchanged with the wave is negligible, the resonance velocity $\Omega_e/k_{||} > \omega_{pe}/k_{||}$ is considerably larger than the electron thermal velocity v_{the}, and the process involves particle energy scattering from the longitudinal direction to the B direction to the transverse direction.

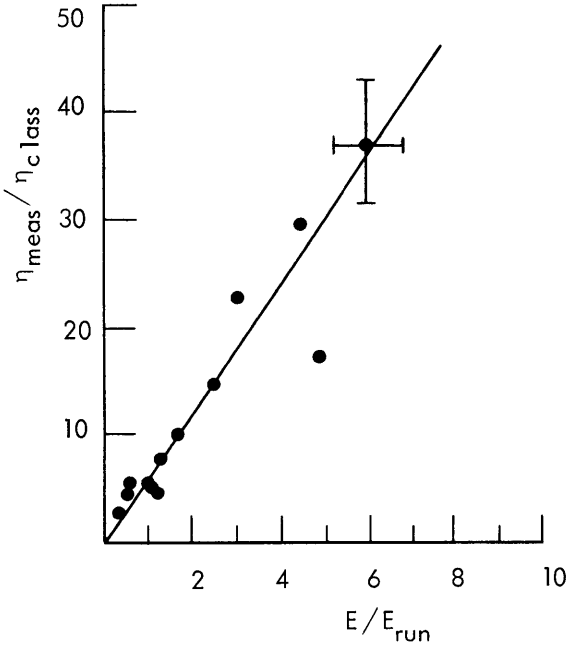

Fig. V-13. Dependence of the relation η_{meas}/η_{class} on E/E_{run} for the TM-3 system

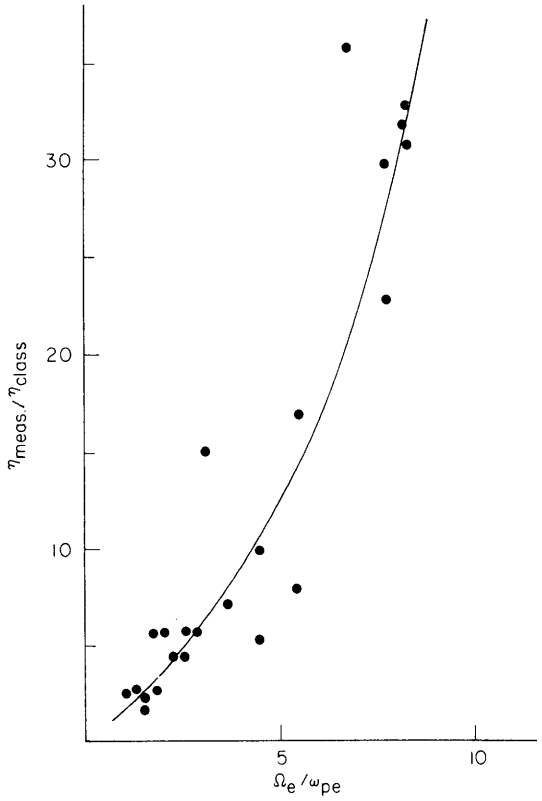

Fig. V-14. Increase of the resistivity anomaly proportional to $(\Omega_e/\omega_{pe})^3$.

It was suggested that two temperatures should be considered: a longitudinal temperature that is to be associated with the measured resistivity and a transverse temperature, the longer, to be associated with the group of fast particles resulting from the scattering of run-away electrons. We recall that Figs. V-13 and V-14 were reported at the 1968 Novosibirsk Conference.[3] In particular, Fig. V-2 showed an increase of the resistivity anomaly proportional to $(\Omega_e/\omega_{pe})^3$ that was consistent with the model of Kadomtsev and Pogutse.[2]

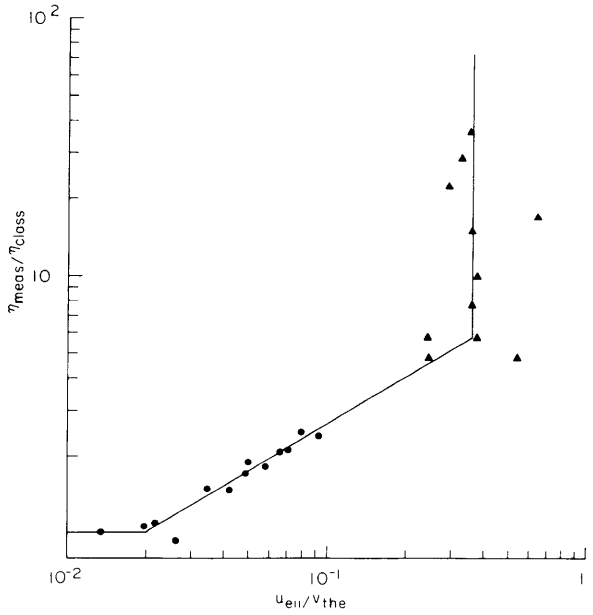

Fig. V-15. Evidence of anomalous resistivity as a function of electron current. Here η_{meas} is the ratio of the applied electric field to the average current; η_{class} is the resistivity evaluated from the classical Spitzer formula as a function of the measured electron temperature $T_{e\perp}$ and averaged over the plasma cross section; $u_{e\perp}$ is the average electron flow velocity along the magnetic field, and v_{the} the electron thermal velocity. The dot points refer to an experiment carried out on the Princeton C-Stellarator, where the electron temperature was evaluated by light laser scattering. The triangular points refer to experiments carried out on the TM-3 Tokamak device, where the electron temperature was obtained by diamagnetic measurements.

At that time, work was being carried out on the interpretation of the anomalous resistivity that had been observed on the Princeton Stellarator. In this case the considered electric fields were much smaller than the run-away field, Ω_e was generally larger than ω_{pe}, and the electron temperature transverse to the field was measured by laser light scattering as the width of the electron distribution function.

A comparison of the results for the TM-3 device and of some of those for the Stellarator was given in Fig. V-15, showing the relative resistivity anomaly as a function of the ratio $u_{e\parallel}/v_{the}$, where $u_{e\parallel}$ is the electron flow velocity along the field, and v_{the}

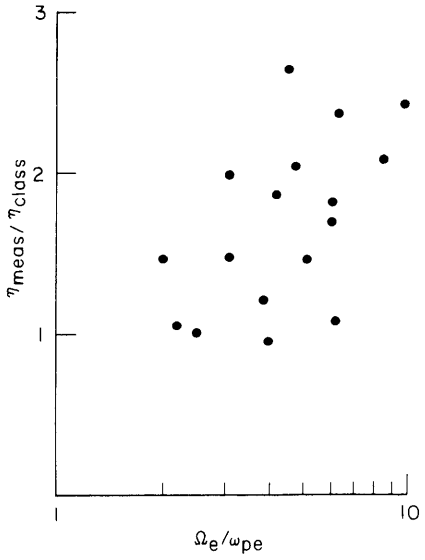

Fig. V-16. Evidence of lack of relationship between η_{meas}/η_{class} and ω_e/Ω_{pe} in stellarator experiments.

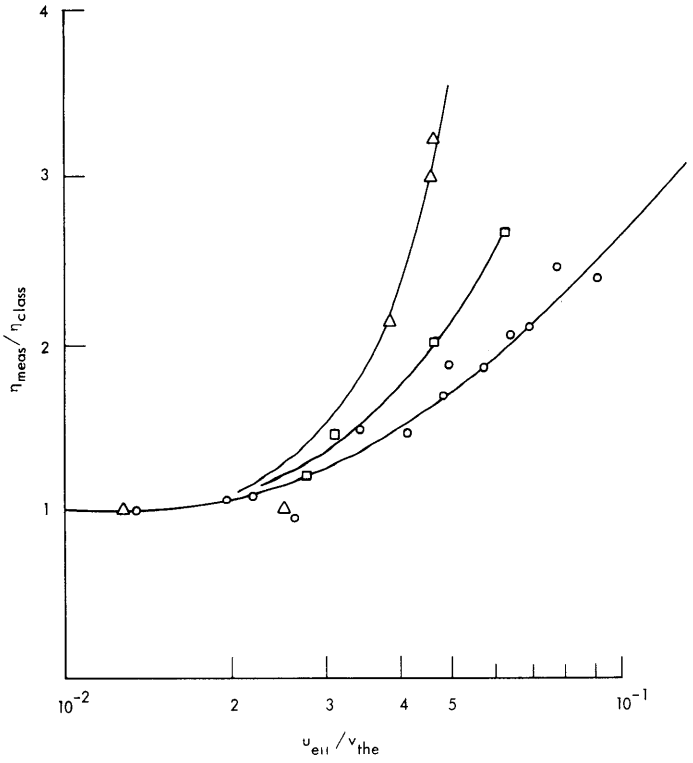

Fig. V-17. Evidence of magnetic field dependence of anomalous resistivity for u_e/v_{the}.

He^{++} Sirius (Kharkov) Stellarator.

H^+ 35 kG, H^+ 17.5 kG } C-Stellarator.

is the electron thermal velocity. The remarkable feature is that two distinct regimes are evident. The one corresponding to the TM-3 experiments shows that the electron flow velocity reaches a saturation value at $\sim 1/3\ v_{the}$, so that the resistivity anomaly increases linearly with the ratio E/E_{run}. The regime corresponding to the lower electron flow velocities for the Stellarator shows a milder dependence of the resistivity anomaly on $u_{e\parallel}/v_{the}$, and it can be explained without directly invoking the effects of run-away electrons. In particular, in this regime it is easy to rule out the presence of a temperature anisotropy and a dependence of the resistivity anomaly on the ratio Ω_e/ω_{pe} is difficult to identify (Fig. V-16).

On the basis of the results available for the T-3 experiments well before the Dubna conference,[4] we argued that the typical regime to which these could be ascribed was similar to that of the first part of the anomalous resistivity curve analyzed on the C-Stellarator. To explain the anomalous resistivity in this regime, a double electron anisotripic temperature model was quite improbable. In fact, if in comparison, we consider the Stellarator experiments, we can see that the magnetic field dependence of the resistivity anomaly is of the form B^{-a}, with $0 < a < 1$ (Fig. V-17), while a mechanism relying on the scattering of run-away electrons would probably lead to a growing function of B, as pointed out by Kadomtsev and Pogutse.[2] Also, theoretical work carried out in collaboration with Kulsrud, Oherman, and Spight had shown that the growth rate of the instability, corresponding ot the resonance, Eq. 1, was weak and very sensitive to the value of the electron collision frequency.

In comparing the amount of anomalous resistivity observed for Stellarator plasmas with temperatures $50\ \text{eV} < T_e < 200\ \text{eV}$ with that for Tokamak plasmas with temperatures $T_e \gtrsim 1\ \text{K eV}$, one could argue that in the latter case the resistivity anomaly should be larger for equal values of $u_{e\parallel}/v_{the}$. The reason is that the voltage drop along the plasma column, which is due to electron-ion collisions, decreases strongly as T_e increases. The corresponding voltage drop that is needed to sustain the current in the presence of fluctuations giving rise to the resistivity anomaly, will not decrease as strongly if the fluctuation characteristics (e.g., amplitude and growth rate) are independent of collision frequency.

Taking these matters into account, we had also represented the anomalous resistivity values obtained in the C-Stellarator and in the TM-3 Tokamak as a function of E/E_{run}, as shown in Fig. V-18. This representation was subject to the criticism that, since E/E_{run} is proportional to the electron temperature T_e and η_{cl}^{-1} is proportional to $T_e^{3/2}$, the two indicated regimes would overlap if the Tokamak temperature were overestimated. This criticism was answered by Fig. V-15, however, which showed that since its abscissa $u_{e\parallel}/v_{the} \propto T_e^{-1\ 2}$, the two regimes would be shown to be farther apart if the TM-3 plasma temperatures were underestimated.

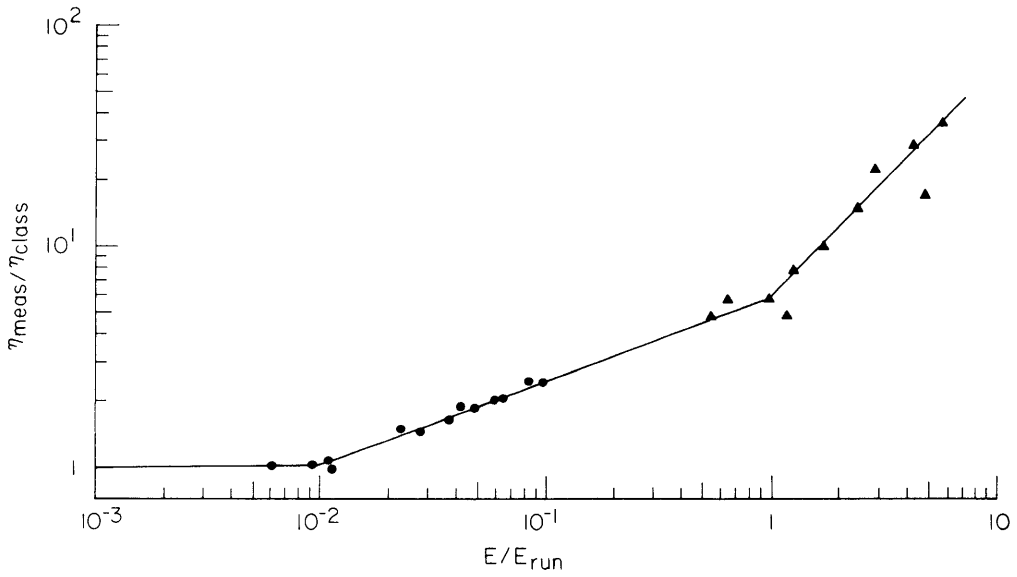

Fig. V-18. Comparison of anomalous resistivity experimental results obtained in Tokamak-confined and C-stellarator-confined hydrogen plasmas as a function of E/E_{run}.

L. A. Artsimovich et al., Third International Conference on Plasma Physics and Controlled Nuclear Fusion Research, Novosibirsk, August 1-7, 1968.
D. Dimock and E. Mazzucato, Phys. Rev. Letters 20, 713 (1968).

The Dubna Conference provided illumination on several of the points discussed above.

1. The Kurchatov team working on the TM-3 device realized that there had been, on their part, a misunderstanding of the magnetic field dependence of anomalous resistivity, due to the fact that temperature and magnetic field B were not varied independently. They recognized[5] that anomalous resistivity in their regime had no appreciable dependence on B, in contrast with what had previously appeared from Fig. V-14.

2. The same team recognized independently that the electron flow velocity reaches a threshold limit of approximately 15 v_s, where v_s is the ion sound velocity (Fig. V-19). This agreed with our finding of the same threshold at ~1/3 v_{the}.

3. Ion heating of the ion distribution tail was found to exist in the same regime where anomalous resistivity occurred. This heating, which cannot be attributed to ion-electron collisions, was shown to decrease as the magnetic field increased (Fig. V-20). Although no detailed work has been carried out to explain the 1/3 v_{the} ceiling of the electron drift velocity, the evidence of anomalous ion heating, which can be associated with ion Landau damping, suggests that ion sound-wave types of mode play an important role in the entire process.

4. Another error of interpretation reported at the Novosibirsk conference was

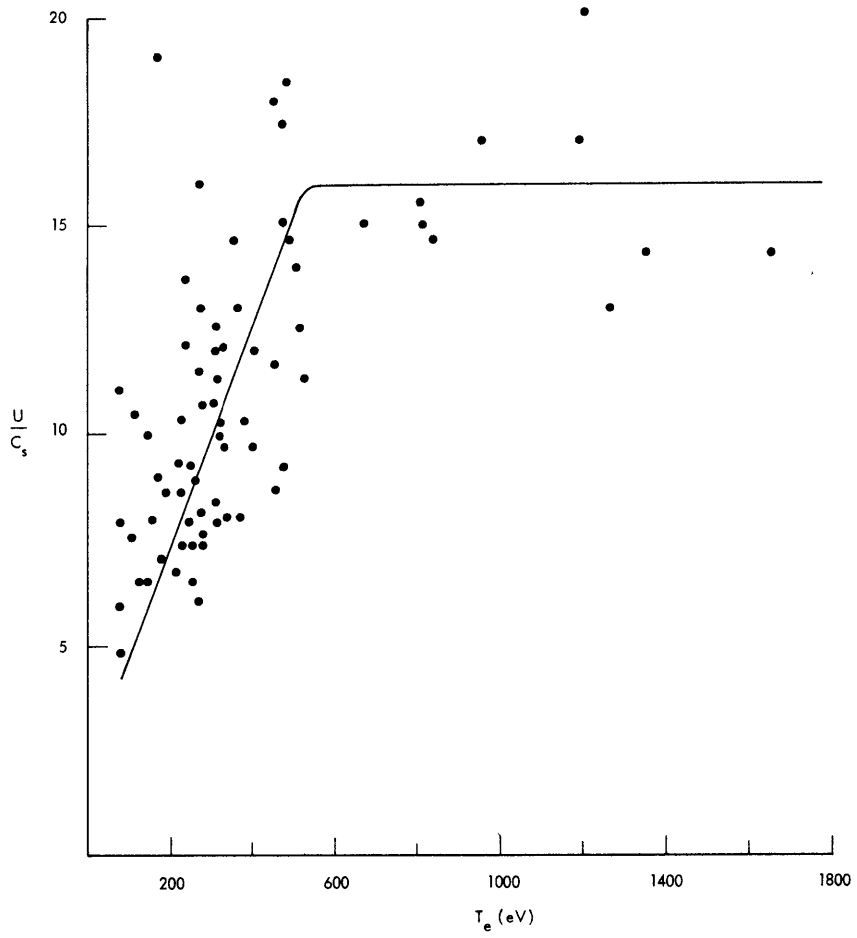

Fig. V-19. U/C_s vs T_e (presented at the Dubna Conference).

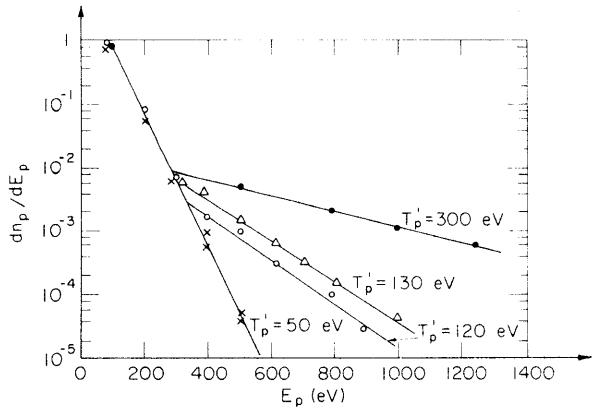

Fig. V-20. Energy spectra of protons for various values of the longitudinal magnetic field under the following conditions.

I = 12 kA, p_o = 3.10 mm HgH_2:

1-H_z = 10 kG; 2-H_z = 14 kG;

3-H_z = 18 kG; 4-H_z = 26 kG.

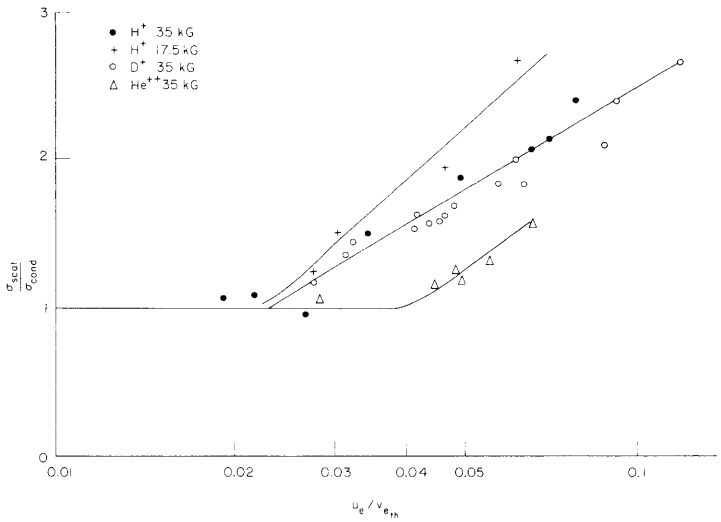

Fig. V-21. Ratio of measured to theoretical plasma resistivity as a function of the ratio of electron drift to thermal velocity.

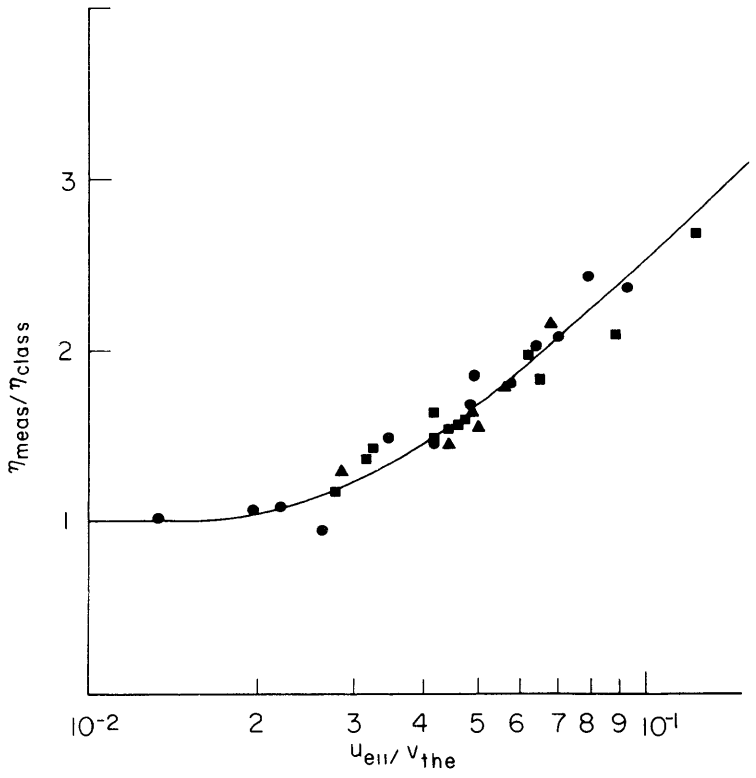

Fig. V-22. Anomalous resistivity for plasmas of different ion mass and charge numbers as a function of U_e/v_{the}

H^+, D^+, H_e^{++} } C-Stellarator, B = 35 kG

straightened out by the time of the Dubna conference. In 1968, Dimock and Mazzucato, in order to test our model of anomalous resistivity in the low electric field regime, carried out experiments in hydrogen and doubly ionized helium. Their results, reported in Novosibirsk, showed that the threshold electron drift velocity $u_{e\parallel}$ above which anomalous resistivity appears in the helium case was about twice that in the hydrogen case (Fig. V-21). This result was hard to reconcile with the above-mentioned model, as it predicted a helium threshold velocity at most as high as that of hydrogen.

Through a re-examination of the experimental data[6] an error of a factor of two was discovered, so that, as indicated in Fig. V-22, the anomalous resistivity curves for hydrogen, deuterium, and helium coincide, which is consistent with the theoretical expectations.

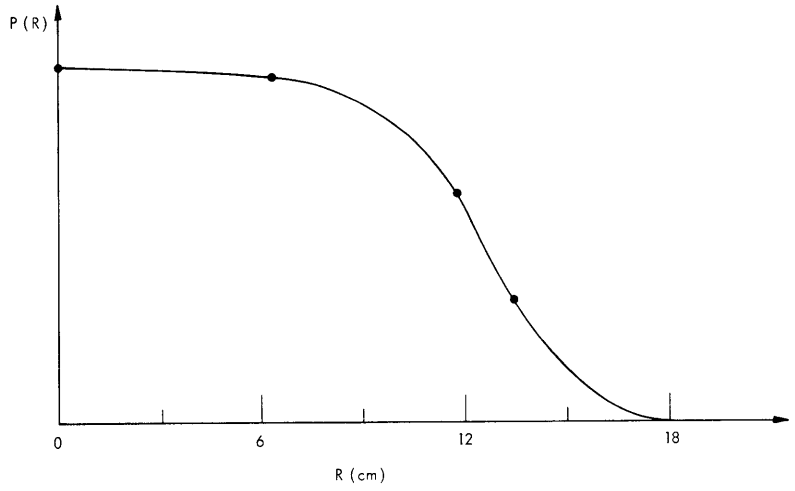

Fig. V-23. Profile of electron pressure $p_e(r) = n_e(r)\, T_e(r)$.

5. With reference to the Tokamak T-3 plasmas, the absence of high-energy electrons and the fact that the temperature is due to the main body of the distribution has been shown unequivocally by the laser light-scattering experiments of the British team.[7]

6. Anomalous resistivity in this regime has been found to occur, but with considerably lower values than in the typical TM-3 regimes and still higher than those observed in Stellarator experiments for equal values of $u_{e\parallel}/v_{the}$. This is consistent with the argument given previously in view of the larger electron temperature in the T-3 plasmas.

7. The measured profile of the electron pressure $p_e(r) = n_e(r)\, T_e(r)$ was shown to be quite flat in the center of the plasma column (Fig. V-23). This is consistent with a model that considers drift modes driven by the electron current along the magnetic field. One expects, in fact, that these modes give rise to anomalous diffusion and tend

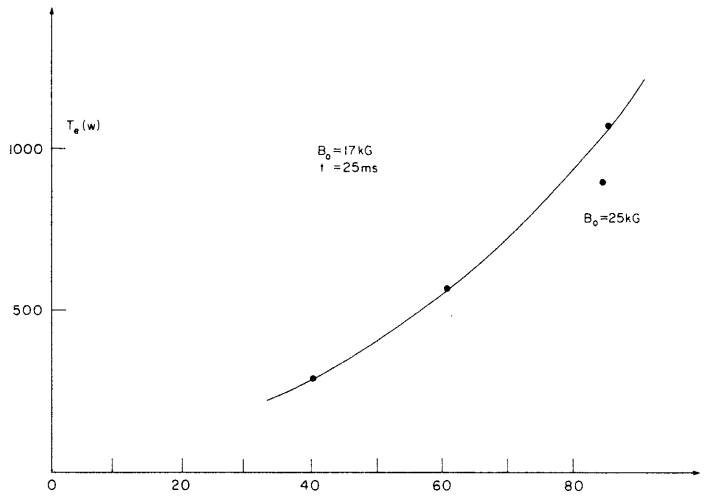

Fig. V-24. Presented at the Dubna conference.

to eliminate the gradient of $p_e(r)$ which is at the origin of their instability.

8. A more recent set of measurements has confirmed the above-mentioned finding. More specifically, for a range of current values from 40 kA to 140 kA, the resistivity was found to be larger than classical by a factor of four, while the electron drift velocity was approximately constant about 1.3 v_s. The latter finding can probably be explained by the condition that $\beta_p = 8\pi nkT/B_p^2$ be approximately constant, where B_p is the poloidal magnetic field under which the experiments have been carried out. Thus, if n is held constant, $T_e \propto B_p^2 \propto u_e^2$. This is consistent with Fig. V-24, which was also presented at the Dubna Conference.

An important piece of information is the absence of observed skin effects during the early and late part of the discharge. This result, too, cannot be explained by the simple collisional transport theory and shows the importance of collective modes in determining the effective transport coefficients of high-temperature plasmas.

B. Coppi

References

1. L. A. Artsimovich, G. A. Bobrowskii, C. V. Mirnov, K. A. Razumova, and V. S. Strelkov, Soviet At. Energ. 22, 325 (1967) [Translation from At. Energ. (USSR) 22, 259 (1957)].
2. B. B. Kadomtsev and O. P. Pogutse, Soviet Phys. – JETP 26, 1146 (1968).
3. L. A. Artsimovich, et al., Plasma Physics and Controlled Nuclear Fusion Research, Vol. 1, Conference Proceedings, Novosibirsk, U.S.S.R., 1-7 August 1968 (International Atomic Energy Agency, Vienna, 1969), pp. 157-173.
4. L. A. Artsimovich, Lecture Series on Plasma Toroidal Confinement, Department of Physics, M.I.T., April 1969.
5. G. A. Bobrovoskii, et al., Reprint IAE-1905 (Kurchatov Atomic Energy Institute, Moscow, 1969) [Translation in Report MATT-TRANS-92 (1969), Plasma Physics Laboratory, Princeton University.
6. B. Coppi and E. Mazzucato, Reports MATT-616 (1968) and MATT-720 (1969), Plasma Physics Laboratory, Princeton University.
7. M. J. Forrest, N. J. Peacock, D. C. Robinson, P. D. Wilcox, and V V. Sannikov, Paper presented at the Dubna conference on Toroidal Plasma Confinement, Dubna, U. S. S. R., October 1969.

2. TWO-DIMENSIONAL ANALYSIS OF TOKAMAK FUSION REACTORS

Feasibility of Tokamak reactors is of interest because recent experiments have shown long energy containment times that will be sufficient for reactor purposes if the diffusional scaling holds.[1] The critical β where the plasma becomes unstable and/or equilibrium is lost appears, however, to be rather small and may make economical operation difficult. The purpose of this study is to access the effect of various assumptions about the critical β on reactor operation.

The theoretical maximum β may be written $\beta \sim \frac{\gamma}{q}\left(\frac{a}{R}\right)$, where a and R are the minor and major radii of the focus, respectively, q is the so-called stability margin, and γ is a scale factor to indicate that the critical β may be improved by shaping the magnetic surfaces. The experimentally observed scaling is $\beta \sim \frac{\gamma}{q^2}\left(\frac{a}{R}\right)^2$, however. The operation of future reactors should lie somwhere between these extremes.

The first study of this kind was made by Gibson[2] who assumed the theoretical scaling $\beta \sim \gamma/q^2\left(a/R\right)$ for fixed a and volumetric reaction rate, and pointed out the necessity for high magnetic fields. Golovin et al.[3] adopted the experimentally observed scaling $\beta \sim 1/q^2\left(a/R\right)^2$, and also considered the geometric dependence of the magnetic field when the maximum magnetic field, B_M, is fixed. Both of these analyses are one-dimensional, in the sense that the critical parameters a and R are not allowed to vary freely throughout the analysis.

Tokamak Reactor Model

We assume that the blanket has thickness Δr_b, the superconducting magnet with zero thickness is outside of the blanket, and the maximum magnetic field, B_M, is limited by the current-carrying ability of the superconducting wire. The magnetic field on the axis therefore is

$$B = B_M\left\{\frac{R - (a+\Delta r_b)}{R}\right\}. \tag{1}$$

We also assume that the critical β may be written

$$\beta = \frac{\gamma}{q^2}\left(\frac{a}{R}\right)^n. \tag{2}$$

The volumetric reaction rate for a plasma comprising half tritons and half deuterons becomes

$$P = n_D n_T \langle \sigma v \rangle E_n = 1.0 \times 10^8 \beta^2 B^4 R^* \ W/M^3 \tag{3a}$$

$$R^* = \left\{ \frac{4\langle \sigma v \rangle}{(T_e + T_i)^2} \right\} 0.87 \times 10^{24}, \tag{3b}$$

where E_n is the energy released per fusion (assumed to be 14 MeV, that is, the energy of the fusion neutron) and $\beta \equiv \frac{nk(T_e + T_i)}{\beta^2/2\mu_o}$. D. J. Rose[4] has shown that for $10 < T_i(\text{keV}) < 30$, R^* is a slowly varying function with approximately unit magnitude. Substituting in Eqs. 1 and 2, we obtain

$$P = 1.0 \times 10^8 \ \alpha_{\underline{p}} G(a, R, \Delta r_b, n) \tag{4a}$$

$$\alpha_{\underline{p}} = R^* \gamma^2 (B_M/q)^4 \tag{4b}$$

$$G(a, R, \Delta r_b, n) = 1.0 \times 10^2 \left(\frac{a}{R}\right)^{2n} \left\{ \frac{R - (a + \Delta r_b)}{R} \right\}^4 . \tag{4c}$$

We fix Δr_b at 1 m, which is a value slightly greater than the estimate of Rose. The volumetric power production decreases for small values of a/R and as $R - (a + \Delta r_b) \to 0$. The geometry factor G is a complicated function of a and R, and we have found contour plots of reactor parameters on the a, R plane extremely useful. The scaling with $\alpha_{\underline{p}}$ then gives the scaling with the other independent variables.

Reactor Parameters

Several reactor parameters, such as the total power output and neutron wall flux, can be calculated directly from P by integration over the plasma cross section. The fact that there is a density gradient, that is, that the critical $\beta(r)$ may not be produced, is included via a space factor ϵ. We limit our attention to moderate-sized reactors ($0.5 < a(m) < 4.0$, $3.0 < R(m) < 8.0$).

a. Total Thermal Power Output

The total thermal power output $\mathscr{P} = \epsilon 2\pi a^2 R P$ may be written

$$\mathscr{P} = 1.96 \ \epsilon \alpha_{\underline{p}} \left\{ 10^2 \ a^2 R \left(\frac{a}{R}\right)^{2n} \left(\frac{R - (a + 1.0)}{R} \right)^4 \right\} . \tag{5}$$

Contour plots of $\mathscr{P}$ for n = 2 and n = 1 are shown in Fig. V-25a and V-25b, respectively.

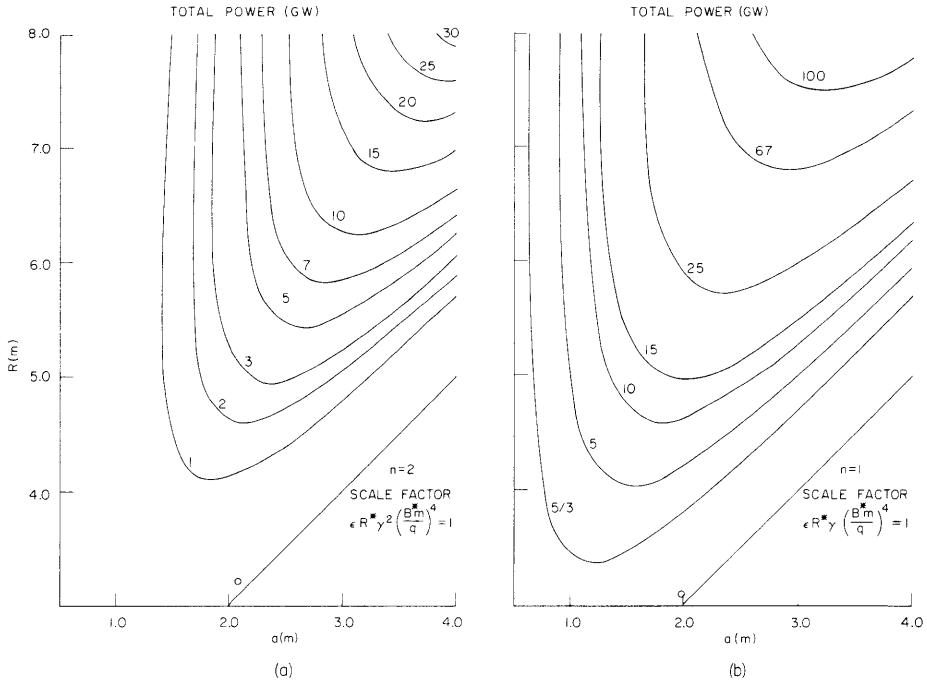

Fig. V-25. Contour plots of $\mathscr{P}$. (a) n = 2. (b) n = 1.

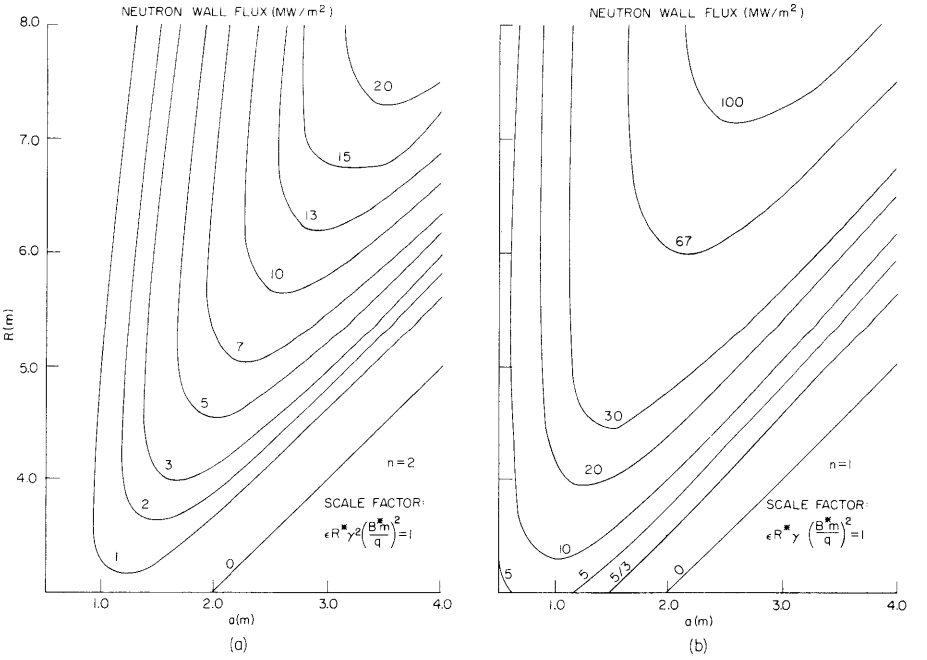

Fig. V-26. Contour plots of F. (a) n = 2. (b) n = 1.

The contour magnitudes are in GW and scale directly with $\epsilon a_{\underline{p}}$. For the experimentally observed scaling n = 2, to obtain thermal outputs in the 2-10 GW range requires roughly $q < B_m$.

b. Wall Flux

The total neutron wall flux $F = \frac{a}{2} P$ may be written

$$F = 50.0\, \epsilon a_{\underline{p}} \left[10^2 \left(\frac{a}{R}\right)^{2n} \left\{ \frac{R - (a + 1.0)}{R} \right\}^4 \right] \frac{MW}{m^2}. \qquad (6)$$

Contour plots of F for n = 2 and n = 1 are shown in Fig. V-26a and V-26b, respectively, and again scale with $\epsilon a_{\underline{p}}$. It is generally agreed that to cool the vacuum wall, F must be less than 10 MW/m^2. For n = 2, if $\epsilon a_{\underline{p}} = 1$ can be achieved, this corresponds to a moderate-sized reactor.

Future Plans

We next plan to study the economics of Tokamak reactors using this technique, and also to investigate other essentially geometric problems such as the maximum temperature obtainable by ohmic heating.

R. A. Blanken

References

1. L. A. Artsimovich, G. A. Bobrovskii, E. P. Gorbunov, D. P. Ivanov, V. D. Kirillov, E. I. Kuznetsov, S. V. Mirnov, M. P. Petrov, K. A. Razumova, V. S. Strelkov, and D. A. Shcheglov, in Plasma Physics and Controlled Nuclear Fusion Research (International Atomic Energy Agency, Vienna, 1969), Vol. I, p. 157; Nucl. Fusion Suppl. (1969), p. 17.
2. A. Gibson, Proceedings of the British Nuclear Energy Society Nuclear Fusion Reactor Conference at Culham Laboratory (to be published).
3. I. N. Golovin, Yu. N. Dnestrovsky, and D. P. Kostomarov, Proceedings of the British Nuclear Energy Society Nuclear Fusion Reactor Conference at Culham Laboratory (to be published).
4. D. J. Rose, Nuclear Fusion 9, 183-203 (1969).